Retrieval of sea ice thickness distribution in the seasonal ice zone from air-borne L-band SAR

Running head: Ice thickness retrieval from L-band SAR

T. TOYOTA*[1], K. NAKAMURA[2], S. UTO[3], K.I. OHSHIMA[1], N. EBUCHI[1]

Affiliation:

1 Institute of Low Temperature Science, Hokkaido University, N19W8, Sapporo, 060-0819, Japan

2 National Institute of Advanced Industrial Science and Technology, 1-1-1, Umezono, Tsukuba, 305-8568, Japan

3 National Maritime Research Institute, 6-38-1, Shinkawa, Mitaka, 181-0004, Japan

E-mail address:

T. Toyota: toyota@lowtem.hokudai.ac.jp

K. Nakamura: nakamura-kazuki@aist.go.jp

S. Uto: uto@nmri.go.jp

K.I. Ohshima: ohshima@lowtem.hokudai.ac.jp

N. Ebuchi: ebuchi@lowtem.hokudai.ac.jp

Abstract

Although it is known that satellite data are useful for obtaining ice thickness distribution for perennial sea ice or in stable thin sea ice areas, it is still an unresolved issue for the seasonal sea ice zone (SIZ). In this study, we approach the problem of ice thickness retrieval by using L-band Synthetic Aperture Radar (SAR). In the SIZ, ice thickness growth is closely related to the ridging activity and therefore surface roughness is expected to be correlated with ice thickness. L-band SAR is suitable for detecting such surface roughness, and therefore is expected to be a good tool for obtaining thickness distribution. To verify this idea, we conducted ship-borne electromagnetic (EM) inductive sounding and supersonic profiling observations with an icebreaker, coordinated with airborne L-band SAR observations in the southern Sea of Okhotsk in February 2005. The surface elevation was estimated by representing the ship's motion with a low-pass filter. Backscattering coefficients correlated well with ice thickness and surface roughness, defined by standard deviation of surface elevation. This result sheds light on the possibility of determining ice thickness distribution in the SIZ.

Keywords

Sea ice; Ice thickness; L-band synthetic aperture radar (SAR); Topography;

Surface roughness; Seasonal ice zone

1. Introduction

The seasonal ice zone (SIZ) occupies about 50% and 80% of the Arctic and Antarctic sea ice extents respectively, and has considerable influence on the climate system (Comiso 2003). Amongst various parameters of the SIZ, ice thickness distribution plays a crucial role in many ways. For example the SIZ usually contains various ice thicknesses and the area fraction of thin ice primarily controls the ocean heat flux to the atmosphere and thus the thermodynamic ice growth rate (Maykut 1978). In terms of sea ice dynamics, thickness distribution determines ice strength, and thus controls ridging/rafting processes and vice versa (Thorndike *et al.* 1975). In addition, its long-term trend provides the evaluation of climate change, as observed for Arctic perennial ice (Rothrock *et al.* 1999; Wadhams and Davis 2000; Tucker *et al.* 2001). Since space-borne remote sensing is an ideal tool for obtaining data on a global scale, enormous efforts have been made to develop an algorithm to retrieve ice thickness distribution. For relatively thin ice, laboratory experiments (e.g., Zabel *et al.* 1996) and field observations (e.g. Kern *et al.* 2006) revealed that active and passive microwave data are useful mainly through the thermodynamic processes that control both ice thickness and surface dielectric properties. Based on these results, the thickness algorithms for coastal polynyas in Arctic and Antarctic regions, combined with NOAA/AVHRR data were also developed (Martin *et al.* 2004; Tamura *et al.* 2007). For perennial ice, the measurement of the freeboard depth has been proved to be effective with the assumption of isostatic balance, from field observations in the Arctic (Comiso *et al.* 1991; Wadhams *et al.* 1992) and from satellite altimetry (Laxon *et al.* 2003; Kwok *et al.* 2004). While the algorithm for stable thin ice or thick perennial ice has been

explored, relatively thick sea ice in SIZ remains a big issue. One of the key problems is validation. It is not easy to obtain *in-situ* ice thickness data covering a wide area at any given time. Recently the electro-magnetic induction sounding technique (EM) has improved our ability to efficiently obtain *in-situ* ice thickness distribution with reasonable accuracy in wide areas (Haas 1998). Another problem is determining which surface property can represent ice thickness distribution. Surface ice salinity becomes less correlated with ice thickness for ice thicker than about 0.5m, suggesting that passive microwave sensors are not necessarily a robust tool. Additionally, the freeboard in the SIZ (mostly less than 0.2 m) is generally too small to be accurately estimated from satellite altimetry. Alternatively the degree of surface roughness can be considered as a useful surface property because deformation processes in the SIZ, usually accompanied by surface roughness, play an essential role in the increase of ice thickness (Worby *et al.* 1996; Toyota *et al.* 2007). To extract surface roughness, the backscatter coefficient of SAR data with a wavelength of the same order as the scale of the roughness on ridges is useful (Massom 2006). In this context, L-band SAR (wavelength = 0.15-0.30 m) data appears to be more suitable for this purpose, in contrast to the C-band (wavelength = 0.03-0.07 m) data that has been mainly used for satellite SAR so far. As a preliminary experiment of ALOS/PALSAR (L-band SAR, launched in 2006), airborne Pi-SAR observations (X- and L-band) were performed in the southern Sea of Okhotsk in February 2005, where conditions were typical of a SIZ. Taking this opportunity, we conducted ship-based measurements of ice thickness and surface roughness in this region with the patrol vessel *P/V* Soya, coordinated with the airborne Pi-SAR observations. Although the relationship between ice thickness and L-band SAR

backscatter data has been studied by several researchers (e.g., Nakamura *et al.* 2005; Kern *et al.* 2006), most concentrate on relatively thin ice (<1m). Based on previous Pi-SAR observations in the same region, conducted in February 2000, Wakabayashi *et al.* (2004) and Matsuoka *et al.* (2002) discussed the relationship between the IPS (Ice Profiling Sonar) ice-draft data and L-band SAR backscatter coefficients for about 1m thick ice. However, ice thickness was not a direct measurement at that time and the relationship with surface roughness was not examined quantitatively. Although Ishizu *et al.* (1998) estimated surface profiles of sea ice using an airborne laser profiler in the same region, ice thickness was not measured. During the ICEX'92 experiment, Malinas and Shuchman (1994) examined the relationship between C-band & L-band SAR backscatter and ice draft for ice thicker than 2 m in the Lincoln Sea. However, surface roughness was not measured at that time. Therefore this Pi-SAR experiment provided us with the first opportunity to compare ice thickness, surface roughness, and SAR backscattering coefficients. To validate the ice thickness data of the EM sensor, calibration was also conducted by ice drilling on another day during the cruise. The purpose of this paper is to examine whether the degree of surface roughness can be a good tool for obtaining ice thickness distribution in the SIZ and to investigate the feasibility of L-band SAR data on the basis of observational results in the Sea of Okhotsk. Since it has been shown that sea ice growth processes in this area have similarity to those in the Antarctic Seas (Toyota *et al.* 2007), we believe that our results can be applied to the general SIZ.

2. Measurements

This field experiment was carried out in the southern Sea of Okhotsk on February 14, 2005 to compare airborne L-band SAR backscattering data with ship-borne measurements of ice thickness and surface roughness along the ship track. This area is usually covered with sea ice from January to April and the period of this observation corresponds to ice growth season, close to its maximum extent. Conducting hourly visual observations using ASPeCt protocols (Worby *et al.* 1999), the undeformed ice thickness ranged from 0.3 to 0.7 m with an average of 0.33 m, and the total average ice thickness, including ridged ice area fraction (26%), was estimated to be 0.84 m (Toyota *et al.* 2007). The dominant ice floe size was less than 20 m (35%), followed by new sheet ice (26%) and floes between 20 to 100 m (22%). Along the observation line of this study, our ship was forced to return back due to heavy sea ice after completing half of the original plan.

The aircraft flew over the study area from 12h00m to 12h03m (JST) on February 14, then headed to the coastal region of Hokkaido before finally returning to Hakodate Airport in southern Hokkaido. Coordinated with these observations, ground truth data of ice thickness and surface roughness were obtained in the same region using the patrol vessel *P/V* SOYA. The observation line of the vessel was about 40 km long, located about 50 km off the coast of Hokkaido (figure 1). A video camera was mounted on the ship's mast to record the ice conditions in front of the ship during the experiment. The position of the ship was recorded by a Global Positioning System (GPS) unit at an interval of 10 seconds. The ship's track and one of the observation areas surveyed from the aircraft are shown in figure 1.

2.1 Pi-SAR

Pi-SAR, developed jointly by the Japan Aerospace Exploration Agency (JAXA) and the National Institute of Information and Communications Technology (NICT), collects fully polarimetric data in both L- and X-bands. This study concentrates on the L-band polarimetric backscattering coefficients because our main interest is to relate them to ice-surface roughness at the scale of ridging. For L-band, the centre frequency is 1.27 GHz (wavelength = 0.24 m) and the incident angles are 39.9, 31.7 and 46.5 degrees at the centre, near edge, and far edge of the image respectively. The dependence of L-band SAR backscattering coefficients on incident angles is known to be quite small within this range, irrespective of the sea ice surface (Wakabayashi *et al.* 2004). The horizontal resolution is 3 m, and the original data were smoothed spatially with a running mean over 3x3 pixels to reduce the scatter inherent in the data due to small-scale sea ice heterogeneities and instrument noise.

2.2 Ice thickness

Ice thickness was monitored with a ship-borne EM system. This system was composed of an EM instrument (EM31/ICE, Geonics Ltd.) and a laser profiler (LD90-3100HS, Riegl). The former measures the height of the EM instrument above the seawater surface (i.e. ice bottom) using electromagnetic induction, while the latter measures the height of the laser profiler above the snow or ice surface. By subtracting the height of the instrument above the ice from the distance to the seawater surface, the ice thickness data can be estimated. To avoid any electrical interference, the EM system was fixed in a

wooden frame and suspended below a 7 m long boom extended from the left side of the hull, at a height of about 4 m above the ice surface (figure 2). The footprint of the EM sensor, which is known to be 1.3 times the instrument height above the water surface (Haas 1998), is estimated to be 5 m. Data was sampled at 10 Hz and then averaged and logged on a personal computer every 2 seconds, corresponding to about 10 m resolution. The output of the EM instrument was calibrated by checking the change in height when lifting and lowering the instrument over ice, nilas, and seawater during the cruise in 2004 and 2005. While the EM system was shown to be suitable for Antarctic sea ice, there are still uncertainties in transforming the EM outputs to determine ice thickness over deformed ice due to seawater-filled gap layers between ice blocks (Haas 1998; Worby *et al.* 1999). These layers significantly alter sea ice conductivities and affect the estimation of ice thickness. Therefore a new algorithm was designed for this region to transform the output of the EM instrument to ice thickness based on the drilling calibrations on specific ice floes and subsequent ice core analysis. At the calibration, three ice floes of 2.24, 2.48, and 2.05 m thick containing seawater- or slush-filled gap layers were selected, and the algorithm takes into account the effect of such layers, assuming that they appear periodically within the ice. The accuracy of the model for ridged ice is estimated to be 0.24 m from the root-mean-square error of the calibrations. The details of this algorithm are described by Uto *et al.* (2006).

2.3 Surface roughness

The surface roughness was monitored with a supersonic profiler (UD-390, KEYENCE) mounted to a ladder installed at the bow (7.4 m above sea level, see figure 3(a)), which

measured the height of the profiler sounder above the snow or ice surface at a sampling rate of 7.7 Hz. The electric current output was converted to distance by a specific linear regression. The vertical resolution of the measurement is estimated to be 0.03 m. The footprint on the ice surface is 0.2 m and the response time is 0.13 seconds. To reduce the noise caused by wind or small scale fluctuations, the averaged values for the previous 10 points of data (1.3 seconds), corresponding to approximately 6 m, were recorded on a data logger at the interval of 0.1 second. The raw data is significantly affected by the vertical motion of the ship, and it is therefore important to know the properties of the ship's motion. For this purpose, two of the same profilers were also mounted on either side of the ship's forecastle (figure 3(b)). These three sounders were kept in the nadir direction using a gimbaling system and the data was recorded on the same data logger to synchronize the measurements.

3. Methods of Analysis

3.1 Segmentation of ship track for analysis

Since the relationship between surface roughness, ice thickness, and SAR data may depend on ice conditions such as ice concentration, floe size, and thickness, it is desirable to compare them under similar ice conditions. The ship's motion which significantly affects the profiling data also seems to depend on the ice conditions. Therefore, lines on which similar ice conditions continue consecutively were selected from the full ship track for analysis with the video images from the front view. In selecting these lines, the following criteria were also taken into account: 1) the duration of observations was more than 5 minutes, and 2) the ship was proceeding straight ahead

at a constant speed because changes in speed or direction can alter the ship effect. As a result, seven lines were selected. Their positions are shown in figure 1 and the ice conditions are listed in table 1.

3.2 Surface roughness

To extract surface elevation from the supersonic profiler data which has a large variability associated with the ship's motion, it is essential to determine the sea levels at each point. For this purpose it is requisite to know the properties of ship motion. In previous studies using airborne observations of Arctic sea ice (e.g., Hibler 1972), the sea level was manually extracted at several local minimum points and then the overall sea level was estimated by interpolating between the extracted points. However in the case of the Okhotsk sea ice, where ice thickness is relatively thin compared to thick perennial Arctic ice, a more precise estimation method for determining sea level is needed. In this study we used a statistical method following Ishizu *et al.* (1999). We began by examining the properties of the ship's motion under the conditions of no sea ice or with only thin nilas. Generally there are three kinds of motion which can affect the profiling data: rolling, pitching, and vertical oscillation due to buoyant force. The period of vertical oscillation is estimated to be 3.8 second from the following formula, assuming a rectangular shape for the ship:

$$T = 2\pi\sqrt{\frac{M}{\rho_w \cdot g \cdot S}} \quad ,$$

where M and S denote the mass and basal area of the ship respectively, and ρ_w is the seawater density. The periods of rolling and pitching were estimated from the three

profiling datasets. The difference in height between the right- (R) and left- (L) side data represents the rolling motion, while the difference between their average (R+L)/2 and the bow (F) represents the pitching motion (figure 3(b)). The pitching and rolling components were usually compounded, making it difficult to evaluate the individual properties, and only three minutes of data could be found where an inverse correlation between R and L was clear (figure 4(a)). Since both components are considered to be independent during this period, the spectral peaks of R-L and F-(R+L)/2 provide the representative periods of rolling and pitching, which are approximately around 9 and 6 seconds respectively (figure 4(b) and (c)). Obviously in this case the power spectrum of F exactly coincides with that of the pitching motion (figure 4(d)).

Next, we examined the ship's motion over the ice covered area. The typical power spectra of F, calculated for various floe sizes, are shown in figure 5. In the real ice area, the interaction between ice floes and the ship's motion produces some deviation from the inherent periods above. Although they have rather broad bands, it is shown that two prominent peaks appear at about 5 and 10 seconds, probably corresponding to the pitching and rolling motion. In addition it is noticed that in most cases, irrespective of ice conditions, the power spectrum shows a different pattern above and below the period of about 2 seconds and significantly increases for periods longer than 2 seconds. This indicates that the variability of the profiling data due to the ship's motion and surface roughness occur on different time scales and that the former can be represented by low-pass filtering. In this study we used a Lanczos-cosine filter with a cut-off period of 2 seconds, corresponding to approximately 10 m. Since the horizontal scale of surface roughness appeared to be mostly less than 10 m, this filtering appears to work

effectively to detect the ship's motion with the exception of significantly ridged areas. Thus the time series of filtered data, hereafter referred to as *sm*(t), are considered to represent the ship's motion as well as the mean ice levels.

The second step is to obtain the sea level at each point. A standard deviation *sd(t)* from *sm(t)* was calculated for a time segment of ±2 seconds each block of data containing 41 data points. Here the key point is that the data above *sm(t)* were neglected and only the data below *sm(t)* were used for the calculation of *sd(t)* (Ishizu *et al.* 1999). This serves to exclude the data associated with extremely high ridges. The time series of *sd* were also low-pass filtered in the same way. Assuming that surface roughness lower than *sm(t)* follows a Normal distribution, $sm(t) \pm 1.5 \times sd(t)$ is estimated to contain all data at a significant level of 93 %, and therefore $sm(t) + 1.5 \times sd(t)$, referred to as *ml(t)*, can be regarded as the approximate seawater level. It should be noted that since the time segment for the calculation of *sd(t)* is 4 seconds, *ml(t)* represents the seawater level for ice floes smaller than about 20m, and the surface level of flat ice for those larger than about 20 m.

As a final step, the surface elevation data were obtained by subtracting the original profiling data from the estimated sea level. To represent the degree of surface roughness, we calculated the standard deviation of surface elevation within each 1 km segment and hereafter we define this value as surface roughness. The procedure is summarized in figure 6. The obtained surface elevation data were checked with the front view video images recorded from the ship's mast. When the data showed unrealistically high or negative values, they were excluded as noise. The accuracy is estimated to be about 0.03 m from the fact that the surface elevation over the completely flat nilas area was

0.014 m on average with a standard deviation of 0.011 m. The merit of this method, compared with that of Hibler (1972), is that surface elevation can be obtained simply on a statistical basis. This allows us to extract it to some extent for the sea ice areas where freeboard is as small as the measurement accuracy. However, the problem of this method is to seemingly underestimate the surface elevation overall. The value rarely exceeds 0.1 m, as exemplified by the estimated surface elevation mean in table 1. This will be discussed later. Nevertheless, the degree of roughness almost coincides with the viewed ice conditions and we consider that these data are a suitable parameter of surface roughness.

3.3 Backscattering data

The airborne observations were conducted a few hours after the ship-based measurement and subsequently the observation site was disturbed due to navigation. This means that we cannot directly compare the data point by point. Nonetheless, by considering that similar ice conditions spread out on a scale of a few kilometers, the surrounding sea ice can be substituted for it if we use the statistical properties. In this case we took the lines 200 m away from the selected ship track where ice was undisturbed (figure 7). To make the data more representative, both side lines of the track were adopted and then segmented into 1 km lengths. The SAR data along these segmented lines were used to compare with the ship-based data. Since segmentation was done along the selected ship track, the ice conditions are almost the same within the same segment. It should be noted that the ship track position was not determined from the ship-borne GPS record but from a sequential range of high backscatter coefficients

because the ship tracks had shifted to the south by a few hundreds of meters before the airborne measurement (figure 7). The geological position of each pixel of backscattering data was determined with an Affin Transform from the four corners of the image frame. In this way the backscattering data on the two segments (each side) along the ship track were obtained and then compared with the ship-based ice thickness and surface roughness estimates.

4. Results

There were a total number of 19 segments. The averaged ice thickness ranged from 0.4 m to 1.7 m, which is mostly greater than the thickness of normal level ice in this area (0.3 to 0.5 m; Toyota *et al.* 2004). The scatter plots between surface roughness, ice thickness, and backscatter coefficient averaged along each segment are shown in figure 8. First, figure 8(a) shows a good correlation between the L-band backscatter coefficients and ice-surface roughness (correlation coefficient = 0.80), indicating that the former almost represents the degree of the latter. Next, figure 8(b) shows that ice thickness also correlated well with surface roughness (c. c. = 0.91). This is consistent with the fact that the development of ice thickness, especially for ice thicker than 0.4 m, is controlled by ridging processes in this region (Toyota *et al.* 2007), and indicates that ridging activities are closely related to the degree of surface roughness. Consequently, ice thickness shows a good correlation with the L-band backscatter coefficients with an rms error of 0.19 m (c.c. = 0.88), as seen in figure 8(c). The thickness of the linearly distributed ridges, which cross the ship track from east to west in figure 7, is predicted to be 1.5 to 2 m, using the regression derived from figure 8(c), and this value is in good

agreement with the deformed ice thickness estimated from visual observation (1.99 m; Toyota *et al.* 2007). While the vertical polarimetric data (VV) are used in this figure, the result is almost the same for the horizontal data (HH) (c.c. = 0.85). However, one question may be raised. If our scenario is correct, why does the correlation coefficient of surface roughness with L-band SAR backscatter becomes less than that with ice thickness? Regarding this matter, we consider the theoretical penetration depth of microwave is up to 0.50 m at L-band for first-year ice with the salinity of 5.1 psu (Hallikainen and Winebrenner 1992). Therefore backscattering data is affected by the inner structure of sea ice, which worked to decrease the correlation with ice thickness. Importantly, despite this property the L-band backscatter coefficient corresponds well with surface roughness.

Our result is also consistent with Matsuoka *et al.* (2002). They showed, using airborne SAR data in the coastal region of Hokkaido, that the L-band SAR backscattering profiles had a good correlation with IPS ice-draft, particularly in the thicker regions, although the comparison was indirect in their case. Conversely, the backscattering ratio defined by VV-HH (dB), which reduces the effect of roughness on backscattering and strengthens the dielectric effect (Nakamura *et al.* 2005), has lower correlation with ice thickness (c.c. = -0.77) than either VV or HH (figure 8(d)). This means that surface roughness is better correlated with ice thickness than the brine properties near the ice surface.

To confirm the usefulness of the L-band SAR data, the thickness distribution (probability density) needs to be validated along with the averaged values because we assume that the ice conditions along each segment are similar to those along the ship

track. To this end, the backscatter coefficient at each pixel was converted into an ice thickness, using the regression derived from figure 8(c), and used to calculate the frequency of each ice thickness category along the seven selected lines. The results are individually shown in figure 9. Although the modal values in EM measurement are slightly biased to thinner thickness in some cases, overall the SAR-derived thickness distributions are in good agreement with those from the EM measurements.

Considering that our retrieval method is based on the averaged values, this slight bias seems to be caused by the fact that the SAR-derived thickness distribution does not reproduce the thick ice tail that is observed in the EM data (figure 9). We infer that this is possibly because SAR backscatter data tends to be saturated for high values of surface roughness (figure 8a), which means that L-band SAR backscatter does not correlate well with surface roughness for highly rough surface. There are two possible reasons for this. One is related to the theoretical penetration depth of L-band SAR, which is estimated to be 0.5 to 0.7 m for first-year ice (Hallikainen and Winebrenner, 1992). Since highly developed ice is usually formed through rigorous ridging processes, it can have more complex inner structure compared with thinner ice, which would make the correlation of SAR backscatter data with surface roughness worse. The other reason is related to the vertical ridge profile. According to Tin and Jeffries (2003), about 30% of the ridges seen in the Antarctic sea ice regions are not accompanied by prominent ridge sails. If this were the case for the Sea of Okhotsk, our method would not be available to such ridges and then thick ice tail would be reduced.

Consequently, we conclude as follows: not only the averaged data but also the thickness distribution showed a promising result to some extent. Both indicate that

L-band SAR backscattering coefficients are useful for the retrieval of ice thickness distribution in the SIZ especially for thick ice (>0.4m) which are accompanied by ridging activities. However, we should keep it in mind that the thickness of highly ridged ice may be underestimated by our method.

5. Summary and discussion

In order to exploit the retrieval of ice thickness distribution in the SIZ from space, we examined the potential of surface roughness information from airborne polarimetric L-band radar backscatter data in the southern Sea of Okhotsk in the 2005 winter. To relate the SAR data with surface roughness, the surface topography of sea ice was monitored with supersonic profiling sonar at the bow, coordinated with aircraft observations. At the same time the ice thickness was monitored with a ship-borne EM system for validation. The surface roughness was calculated by taking the standard deviation of the surface elevation data which was obtained by representing the effect of the ship's motion with a low-pass filter. Our analysis showed that these three kinds of data are well correlated with each other, and that ice thickness ranging from 0.44 to 1.65 m can be estimated directly from L-band radar backscattering coefficient with an rms error of 0.19 m. This result can be interpreted as follows: In the SIZ the thickness distribution of relatively thick ice is controlled mainly by ridging activities accompanied by deformation, and therefore the degree of surface roughness corresponds to the ice thickness distribution well.

For relatively thin undeformed ice (less than 1 m), Nakamura *et al.* (2005) showed from a similar experiment in 2004 that ice thickness has a much better correlation with

the VV-HH backscattering ratio than with the backscattering coefficient, contrasting to our result. This indicates that surface dielectric properties are more sensitive to ice thickness for relatively thin ice. This is consistent with the observational result of Toyota *et al.* (2007) in that surface brine volume fraction, which affects the electromagnetic properties significantly at microwave frequencies (Vant *et al.* 1978), has a good correlation with ice thickness especially for ice thinner than 0.50 m and that ridging becomes more important than rafting for ice thicker than 0.40 m. Consequently, all of these results suggest that ice thickness retrieval by L-band SAR is promising for a wide range of ice thickness by virtue of the surface property of dielectric constant for relatively thin undeformed ice and of roughness for thicker ice.

Finally, we would like to mention the analytical method of estimating the surface elevation. Although our method succeeded to some extent in extracting the surface elevation distribution from the profiling data, the problem still remains that the absolute values in table 1 and figure 8 appear to be significantly less than the real topography. There are three possible reasons for this: the accuracy of instrument, the smoothing effect due to averaging, and the technique of low-pass filtering. To check the first and second factor, we conducted a tandem observation of laser and supersonic profilers in the same region in February 2006 and compared the results. A laser profiler, mounted 0.3 m behind a supersonic profiler, recorded the height of the sensor above the ice surface at the sampling rate of 10 Hz without averaging, while a supersonic profiler did it in exactly the same way as in 2005. The results for highly ridged ice conditions (identified in figure 10(a)) are displayed in figure 10(b) and figure 10(c). Except for the noise which frequently appeared in the supersonic data, it is seen that the two profilers

provided almost the same pattern and amplitudes of variation. This is the case for almost the whole period. Therefore, the first and second factors do not seem to be significant. We consider that the low-pass filtering procedure for obtaining the ship's motion might be most responsible for the reduction of surface elevation. The problem is that the large scale ridges whose horizontal scale exceeded 10 m were smoother out by our fitting procedure. Besides the interaction between the ship and the ice floes may have created small-scale fluctuations and made the scales of variation in the ship's motion and surface roughness overlap. The reason that despite this drawback there was a good correlation between ice thickness and backscatter may be because there is some relationship between the horizontal scale of the ridged area and the degree of surface roughness on the scale of the SAR wavelength. We plan to test this idea by measuring surface roughness with a helicopter-borne laser profiler in the same region.

Our investigation indicates great promise for the use of L-band SAR data in the estimation of ice thickness distribution in the SIZ. Since the Phased-Array L-band SAR (PALSAR) data aboard the Advanced Land Observing Satellite (ALOS) has recently become available, it is expected that ice thickness distribution in the SIZ will be obtained in real time on the global scale in the near future.

ACKNOWLEDGMENT

The authors express their sincere thanks to all the crew and scientists onboard P/V *SOYA* for their kind cooperation during the cruise. The Pi-SAR observation in the Sea of Okhotsk was carried out under the Pi-SAR research announcement programme by NICT and JAXA (PI: Prof. F. Nishio). Discussions with Dr. C. Haas, Dr. R. Massom, Prof. H. Wakabayashi, and Dr. S. Aoki, proof-reading by Dr. G. D. Williams, and comments by two anonymous reviewers were also helpful. This study was supported by the fund from Research Revolution 2002 (RR2002) of the Project for Sustainable Coexistence of Human, Nature and the Earth of the MEXT of the Japanese Government, and partly by Grant-in-Aid for Scientific Research (C-18510003).

References

COMISO, J.C., WADHAMS, P., KRABILL, W.B., SWIFT, R.N., CRAWFORD, J.P. and TUCKER, W.B.III, 1991, Top/Bottom multisensor remote sensing of Arctic sea ice, *Journal of Geophysical Research,* **96**(C2), 2693-2709.

COMISO, J.C., 2003, Large-scale characteristics and variability of the global sea ice cover, In *Sea Ice*, D.N. Thomas and G.S. Dieckmann (eds), Blackwell Publishing, pp. 112-142.

HAAS, C., 1998, Evaluation of ship-based electromagnetic-inductive thickness measurements of summer sea-ice in the Bellingshausen and Amundsen Seas, Antarctica, *Cold Regions Science and Technology,* **27**, 1-16.

HALLIKAINEN, M. and WINEBBRENNER, D.P., 1992, The physical basis for sea ice remote sensing, In *Microwave Remote Sensing of Sea Ice*, F.D. Carsey (eds), American Geophysical Union, Washington, DC, pp.29-46.

HIBLER, W.D. III, 1972, Removal of aircraft altitude variation from laser profiles of the Arctic ice pack, *Journal of Geophysical Research*, **77**, 7190-7195.

ISHIZU, M., MIZUTANI, K. and ITABE, T., 1999, Airborne freeboard measurements of sea ice and lake ice at the Sea of Okhotsk coast in 1993-95 by a laser altimeter, *International Journal of Remote Sensing*, **20**(12), 2461-2476.

KERN, S., GADE, M., HAAS, C. and PHAFFLING, A., 2006, Retrieval of thin-ice thickness using the L-band polarization ratio measured by the helicopter-borne scatterometer HELISCAT, *Annals of Glaciology,* **44**, 275-280.

KWOK, R., ZWALLY, H.J. and YI, D., 2004, ICESat observations of Arctic sea ice: first look, *Geophysical Research Letters, **31***, L16401, doi:10.1029/2004GL020309.

LAXON, S., PEACOCK, N. and SMITH, D., 2003, High interannual variability of sea

ice in the Arctic region. *Nature, **425***, pp.947-950.

MALINAS, N.P. and SHUCHMAN, R.A., 1994, SAR derived sea ice thickness during ICEX'92, *Proc. of IGARSS'94,* Vol.3, pp.1756-1758.

MARTIN, S., DRUCKER, R., KWOK, R. and HOLT, B., 2004, Etimation of the thin ice thickness and heat flux for the Chukchi Sea Alaskan coast polynya from special sensor Microwave/Imager data, 1990-2001, *Journal of Geophysical Research,* **109**, C10012, doi: 10.1029/2004JC002428.

MASSOM, R., 2006, Basic remote-sensing principles relating to the measurement of sea ice and its snow cover. In *Polar Remote Sensing, Vol.1: Atmosphere and Oceans*, D. Lubin and R. Massom, pp.356-380.

MATSUOKA, T., URATSUKA, S., SATAKE, M., NADAI, A., UMEHARA, T., MAENO, H., WAKABAYASHI, NISHIO, F. and FUKAMACHI, Y. , 2002, Deriving sea-ice thickness and ice types in the Sea of Okhotsk using dual-frequency airborne SAR (Pi-SAR) data, *Annals of Glaciology*, **34**, 429-434.

MAYKUT, G.A., 1978, Energy exchange over young sea ice in the central Arctic, *Journal of Geophysical Research*, **83**, 3646-3658.

NAKAMURA, K., WAKABAYASHI, H., NAOKI, K., NISHIO, F., MORIYAMA, T. and URATSUKA, S., 2005, Observation of sea-ice thickness in the Sea of Okhotsk by using dual-frequency and fully Polarimetric airborne SAR (Pi-SAR) data,, *IEEE Transactions on Geoscience and Remote Sensing*, **43**, 2460-2469.

ROTHROCK, D.A., YU, Y. and MAYKUT, G.A., 1999, Thinning of the Arctic sea-ice cover., *Geophysical Research Letters*, **26**, 3469-3472.

TAMURA, T., OHSHIMA, K.I., MARKUS, T., CAVALIERI, D.J., NIHASHI, S. and

HIRASAWA, N., 2007, Estimation of this ice thickness and detection of fast ice from SSM/I data in the Antarctic Ocean, *Journal of Atmospheric and Oceanic Technology*, **24**, doi: 10.1175/JTECH2113.1, 1757-1772.

THORNDIKE, A.S., ROTHROCK, D.A., MAYKUT, G.A. and COLONY, R., 1975, The thickness distribution of sea ice. *Journal of Geophysical Research*, **80**, 4501-4513.

TIN, T., and JEFFRIES, M.O., 2003, Morphology of deformed first-year sea ice features in the Southern Ocean. *Cold Regions Science and Technology*, **36**, 141-163.

TOYOTA, T., KAWAMURA, T., OHSHIMA, K.I., SHIMODA, H. and WAKATSUCHI, M., 2004, Thickness Distribution, Texture and Stratigraphy, and a simple probabilistic Model for Dynamical Thickening of Sea Ice in the Southern Sea of Okhotsk. *Journal of Geophysical Research, 109*, C06001, doi:10.1029/2003JC002090.

TOYOTA, T., TAKATSUJI, S., TATEYAMA, K., NAOKI, K. and OHSHIMA, K.I., 2007, Properties of sea ice and overlying snow in the southern Sea of Okhotsk, *Journal of Oceanography*, **63**, 393-411.

TUCKER, W.B., III, WEATHERLY, J.W., EPPLER, D.T., FARMER, L.D., and BENTLEY, D.L., 2001, Evidence for rapid thinning of sea ice in the western Arctic Ocean at the end of the 1980s., *Geophysical Research Letters*, **28**, 2851-2854.

UTO, S., TOYOTA, T., SHIMODA, H., TATEYAMA, K. and SHIRASAWA, K., 2006, Ship-borne electromagnetic induction sounding of sea-ice thickness in the southern Sea of Okhotsk, *Annals of Glaciology*, **44**, 253-260.

VANT, M.R., RAMSEIER, R.O. and MAKIOS, V., 1978, The complex-dielectric constant of sea ice at frequencies in the range of 0.1-40 GHz, *Journal of Applied Physics*, **49**,

1264-1280.

WADHAMS, P., TUCKER, W.B.III, KRABILL, W.B., SWIFT, R.N., COMISO, J.C. and DAVIS, N.R., 1992, Relationship between sea ice freeboard and draft in the Arctic Basin and implications for ice thickness monitoring, *Journal of Geophysical Research*, **97**, 20325-20334.

WADHAMS, P. and DAVIS, N.R., 2000, Further evidence of ice thinning in the Arctic Ocean, *Geophysical Research Letters*, **27**, 3973-3975.

WAKABAYASHI, H., MATSUOKA, T., NAKAMURA, K. and NISHIO, F., 2004, Polarimetric characteristics of sea ice in the Sea of Okhotsk observed by airborne L-band SAR, *IEEE Transactions on Geoscience and Remote Sensing*, **42**, 2412-2425.

WORBY, A. P., JEFFRIES, M.O., WEEKS, W.F., MORRIS, K. and JANA, R., 1996, The thickness distribution of sea ice and snow cover during late winter in the Bellingshausen and Amundsen Seas, Antarctica. *Journal of Geophysical Research*, **101**, 28,441-28,455.

WORBY, A. P., GRIFFIN, P. W., LYTLE, V. I. and MASSOM, R. A., 1999, On the use of electromagnetic induction sounding to determine winter and spring sea ice thickness in the Antarctic, *Cold Regions Science and Technology*, **29**, 49-58.

WORBY, A.P. and ALLISON, I., 1999, A technique for making ship-based observations of Antarctic sea ice thickness and characteristics. Part I: Observational technique and results. *Antarctic Cooperative Research Centre Research Report 14*, 63 pp., University of Tasmania, Hobart, Australia.

ZABEL, I.H.H., JEZEK, K.C., GOGINENI, S.P. and KANAGARATNAM, P., 1996, Search for proxy indicators of young sea ice thickness, *Journal of Geophysical Research*,

101, 6697-6709.

Figure caption

Figure 1. Location map of the observations.

Solid lines denote the observation line selected for analysis.

The small square area corresponds to the frame of figure 7.

Inset: the shaded area corresponds to sea ice extent as of February 15, 2005.

Figure 2. Photograph of the ship-borne electro-magnetic induction sounding (EM) sensor (white ellipse) equipment. The supersonic profilers are also shown at and near the bow (arrows).

Figure 3. Supersonic profiler equipment installed at the forecastle deck.

(a) Photograph of the profilers at the bow (left) and at the right side deck (right)

The sensors were kept in the nadir direction using a gimbaling mechanism.

(b) Schematic picture of their positions with dimensions.

Figure 4. The supersonic profiling data during the period when R and L were inversely correlated. From these data the properties of the ship's motion were estimated.

(a) Original data of R and L

(b) Power spectrum density of rolling motion (R-L)

(c) Power spectrum density of pitching ((R+L)/2-F)

(d) Power spectrum density of F

Figure 5. Power spectrum density for the individual selected observation lines.

(a) No.1 (b) No.2 (c) No.3 (d) No.4

Here four cases with different ice conditions are shown.

See table 1 for the individual ice conditions.

Figure 6. Procedure for extracting surface elevation from the original data.

(a) Time series of original data (dots), mean ice level (broken line), and obtained water level (solid line). Mean ice level was obtained by low-pass-filtering with the cut-off period of two seconds.

(b) Time series of standard deviation from mean ice level, calculated over the period of ±2 seconds for each data.

(c) Extracted surface elevation, which was obtained by subtracting standard deviation from water level.

Figure 7. Distribution of backscattering coefficients in the square area of figure 1, corresponding to No.5 in table 1.

The side length of the square is 5 km. A black line is the ship's track recorded with a ship-borne GPS. Note that this line slightly deviated from the line of high backscattering coefficients, showing that sea ice drifted southward by the time of the SAR observations. Red lines, taken 200 m away from the true ship track, were used for validation.

Figure 8. Scatter plots of the averaged values between

(a) Surface roughness and backscattering coefficient (VV)

(b) Surface roughness and ice thickness

(c) Backscattering coefficient (VV) and ice thickness

The regression is given by $y = 0.170\ x + 3.481$.

(d) Backscattering ratio (VV-HH) and ice thickness

Figure 9. Ice thickness distribution along the individual selected observation lines.

Thick lines denote SAR-derived ice thickness with the regression in figure.8(c).

Thin lines denote EM-derived ice thickness distribution.

Figure 10. Comparison of the measurements between the supersonic and laser profilers, conducted in February 2006.

(a) Ice conditions of the exemplified area (09h05m LST on February 14, 2006).

(b) Example time series of the supersonic profiling data from 09h00m to 09h30m on February 14, 2006.

(c) Example time series of the laser profiling data during the same period.

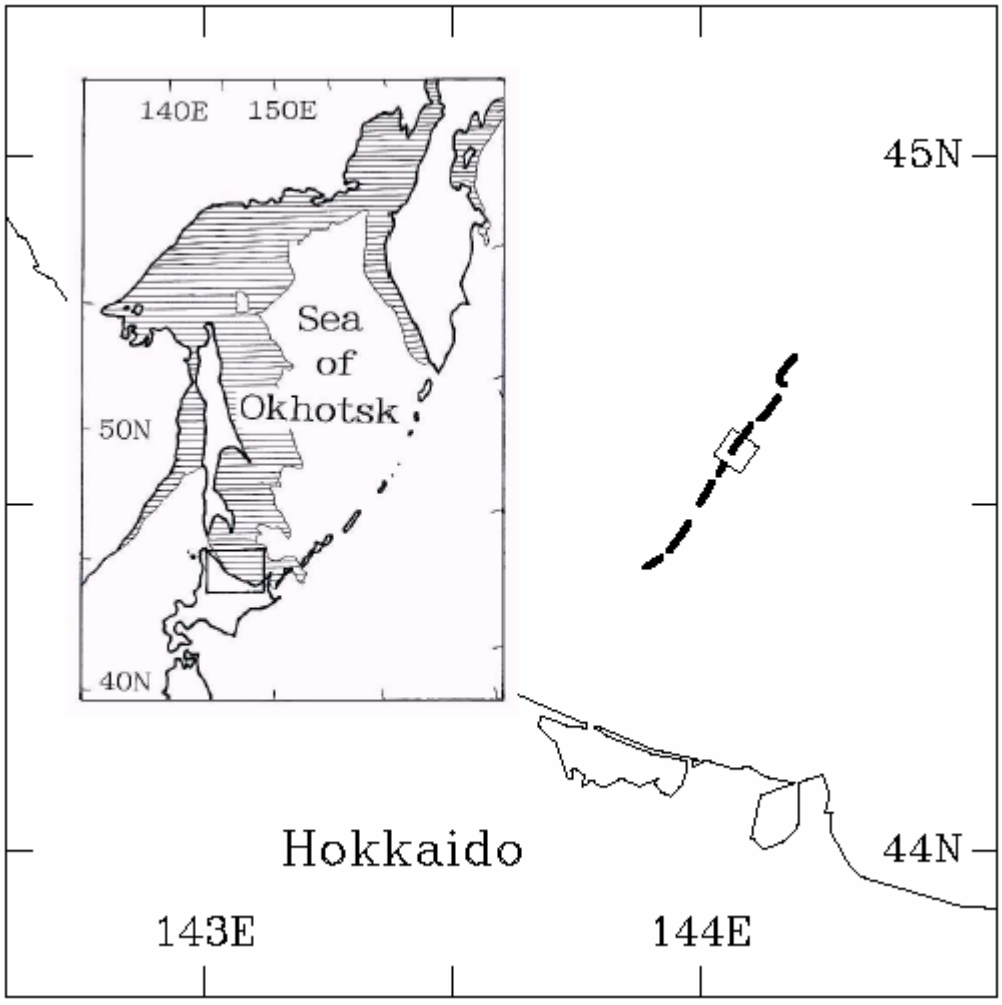

Figure 1. Location map of observation.

Solid lines denote the observation line selected for analysis.

The small square area corresponds to the frame of figure 7.

Inset: the shaded area corresponds to sea ice extent as of February 15, 2005.

Figure 2. Photograph of the ship-borne electro-magnetic induction sounding (EM) sensor (white ellipse) equipment. The supersonic profilers are also shown at and near the bow (arrows).

(a)

(b)

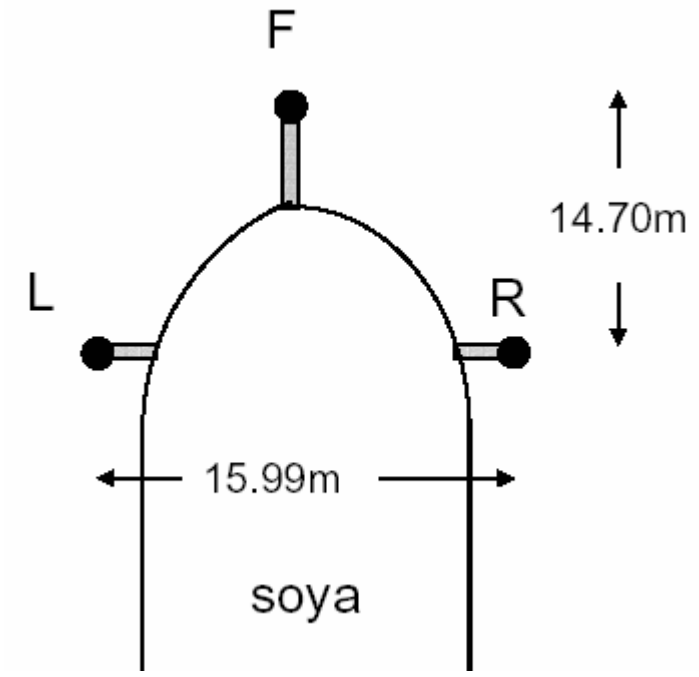

Figure 3. Supersonic profiler equipment installed at the forecastle deck.

(a) Photograph of the profilers at the bow (left) and at the right side deck (right)

The sensors were kept in the nadir direction using a gimbaling mechanism.

(b) Schematic picture of their positions with dimensions.

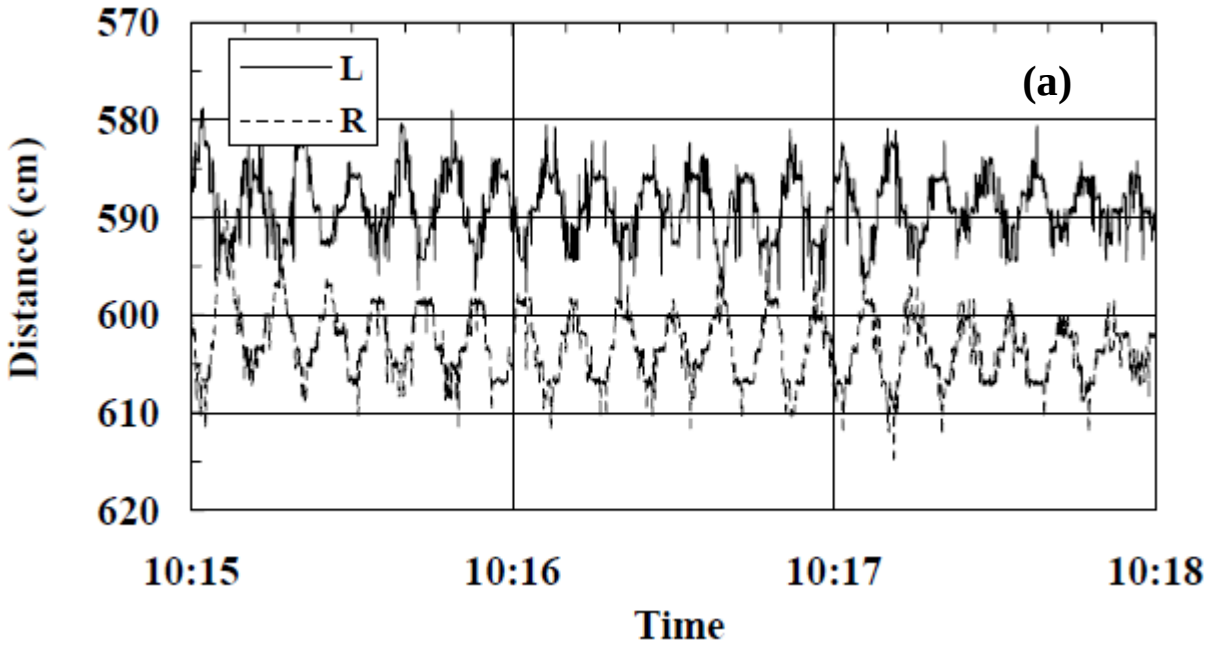
570
580
590
600
610
620
Distance (cm)
L
R
(a)
10:15
10:16
10:17
10:18
Time

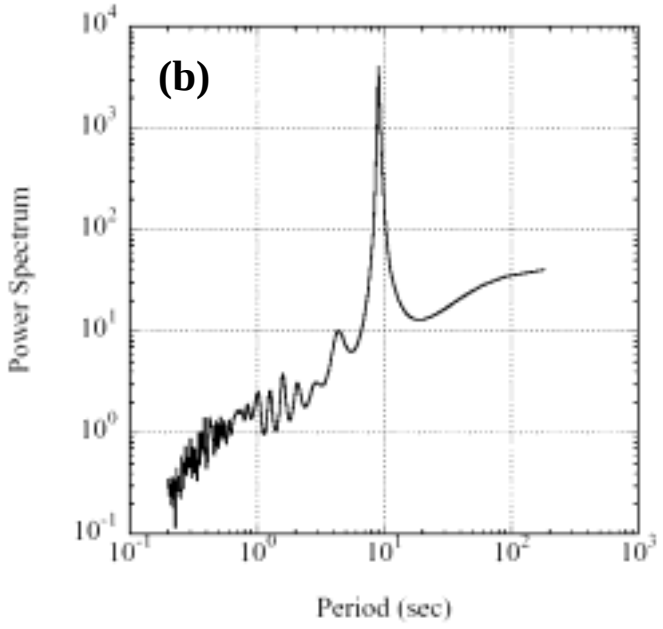
(b)
Power Spectrum
Period (sec)

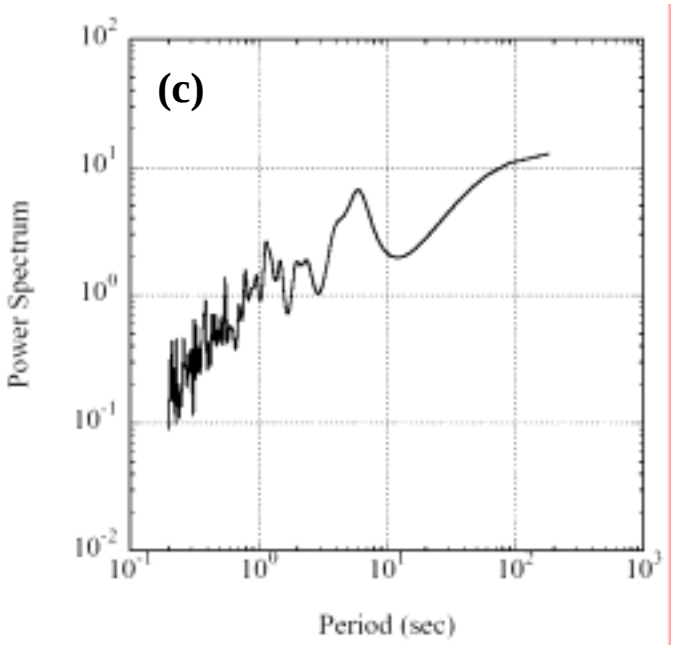
(c)
Power Spectrum
Period (sec)

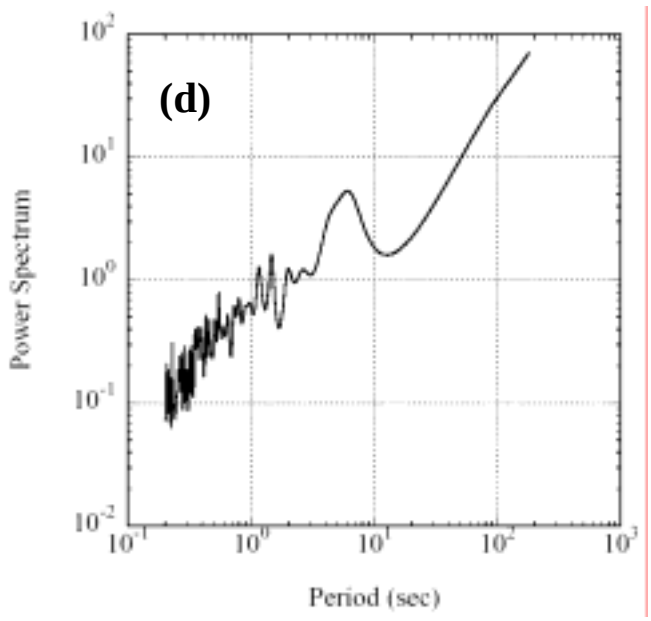

Figure 4. The supersonic profiling data during the period when R and L were inversely correlated. From these data the properties of ship motion were estimated.

(a) Original data of R and L

(b) Power spectrum density of rolling motion (R-L)

(c) Power spectrum density of pitching (F-(R+L)/2)

(d) Power spectrum density of F

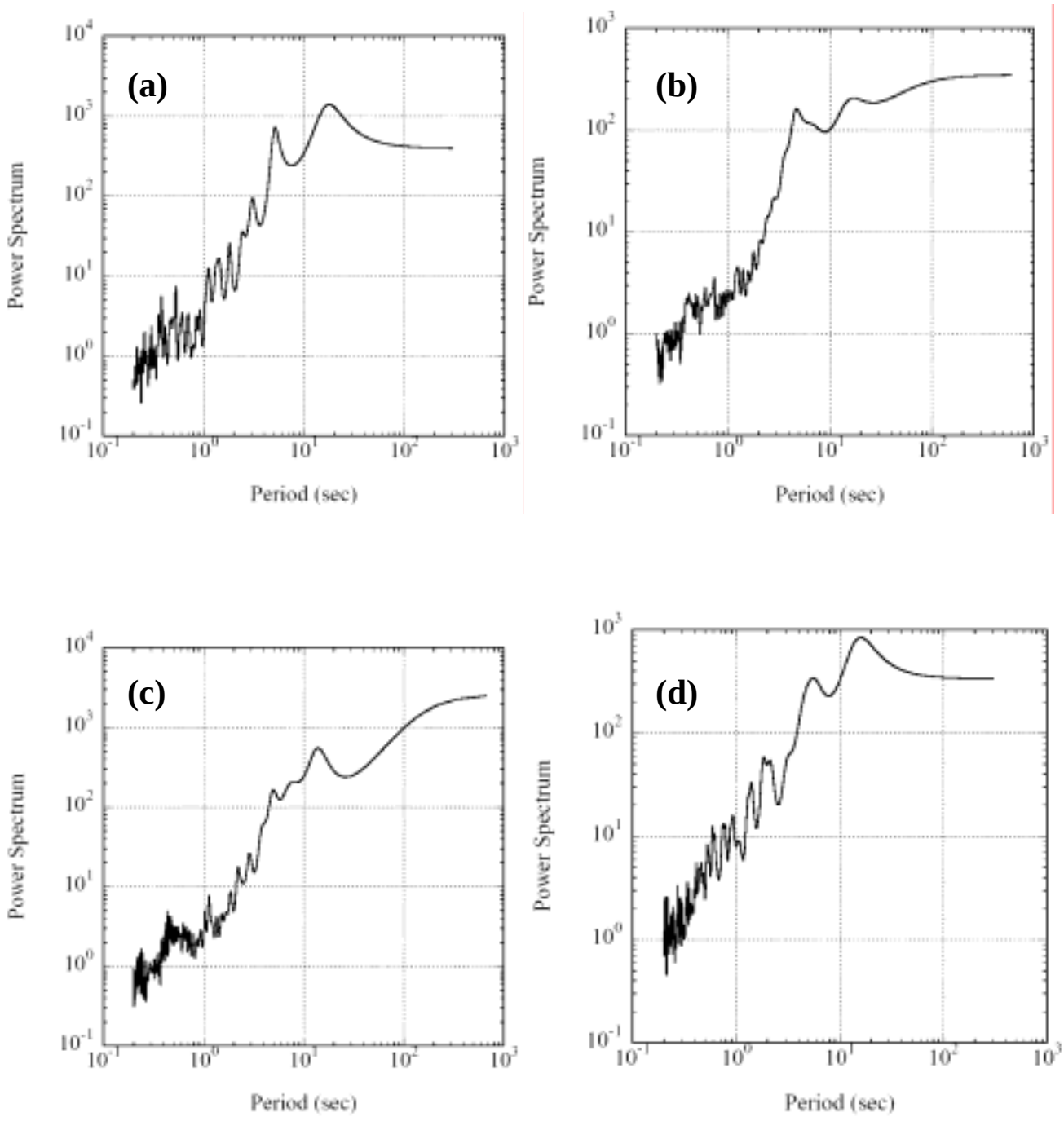

Figure 5. Power spectrum density for the individual selected observation lines.
(a) No.1 (b) No.2 (c) No.3 (d) No.4
Here four cases where ice conditions were quite different are shown.
See table 1 for the individual ice conditions.

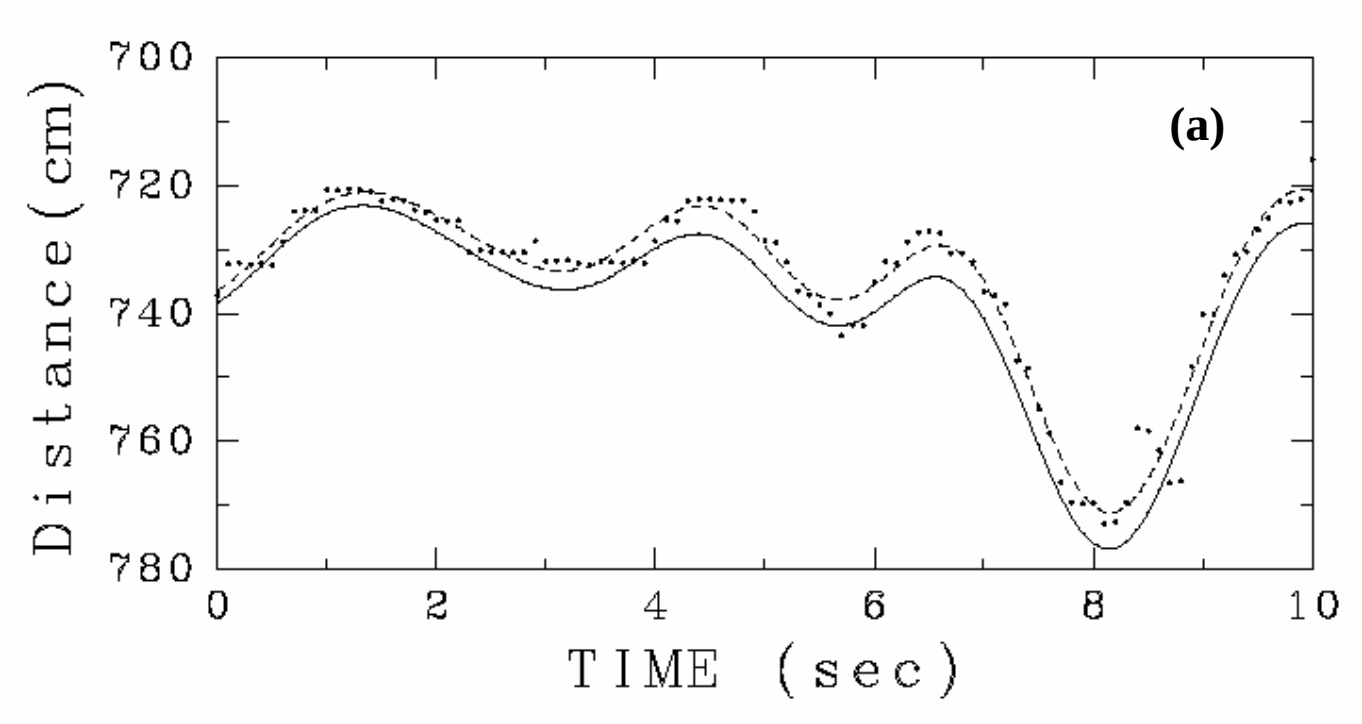
(a)
Distance (cm)
700
720
740
760
780
0
2
4
6
8
10
TIME (sec)

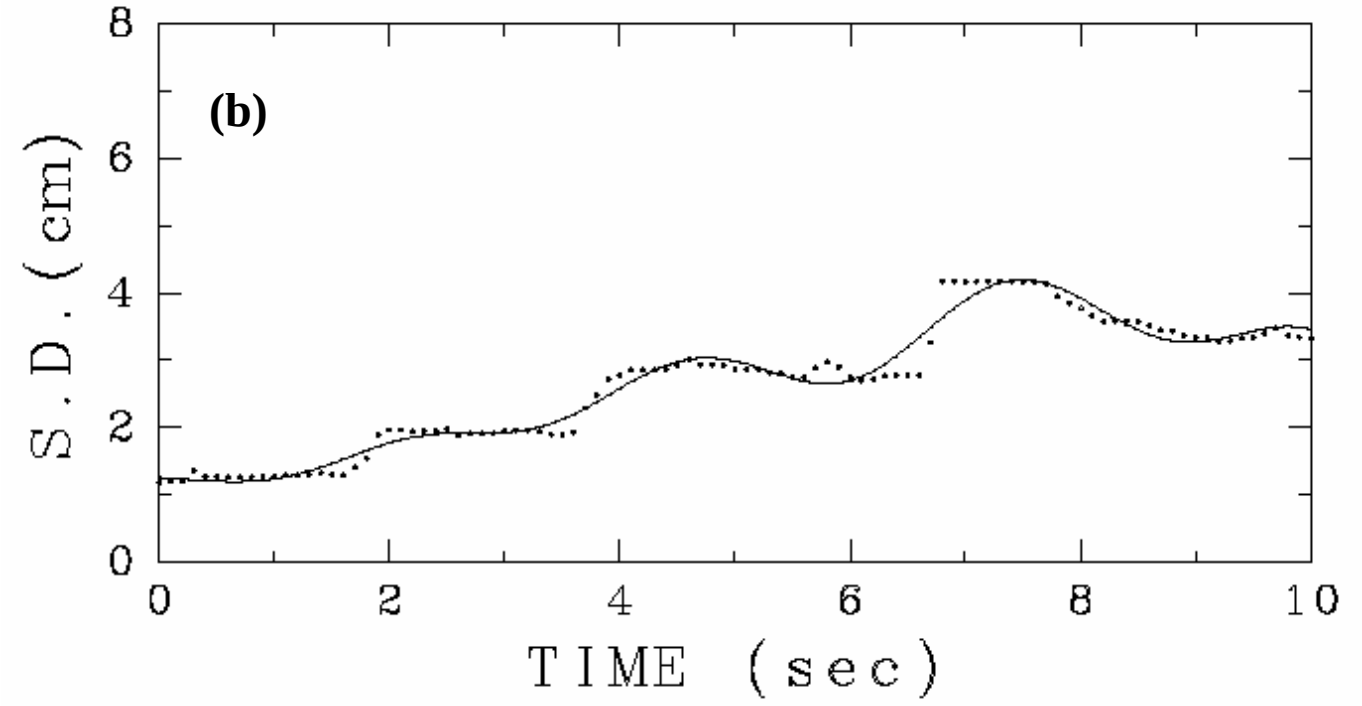
(b)
S.D. (cm)
0
2
4
6
8
0
2
4
6
8
10
TIME (sec)

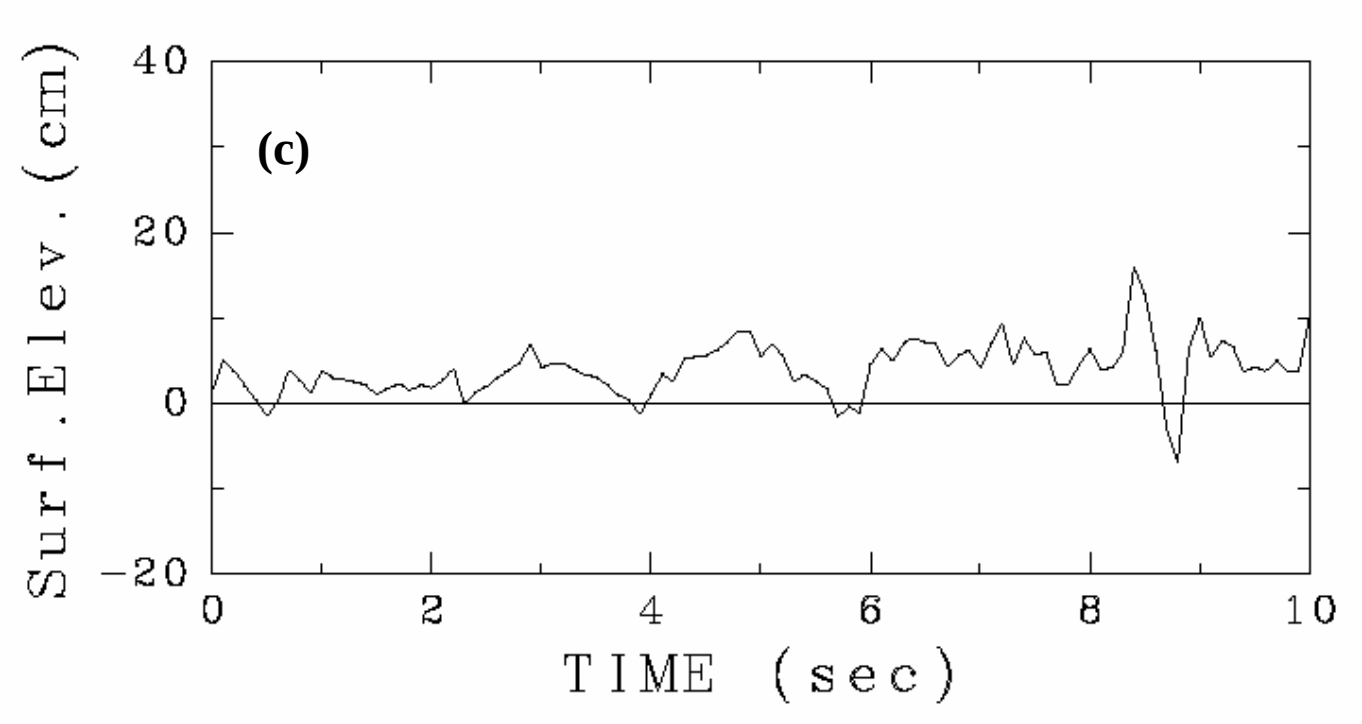

Figure 6. Procedure to extract surface elevation from the original data.

(a) Time series of original data (dots), mean ice level (broken line), and obtained water level (solid line). Mean ice level was obtained by low-pass-filtering with the cut-off period of two seconds.

(b) Time series of standard deviation from mean ice level which was calculated within the period of ±2 seconds for each data.

(c) Extracted surface elevation, which was obtained by subtracting standard deviation from water level.

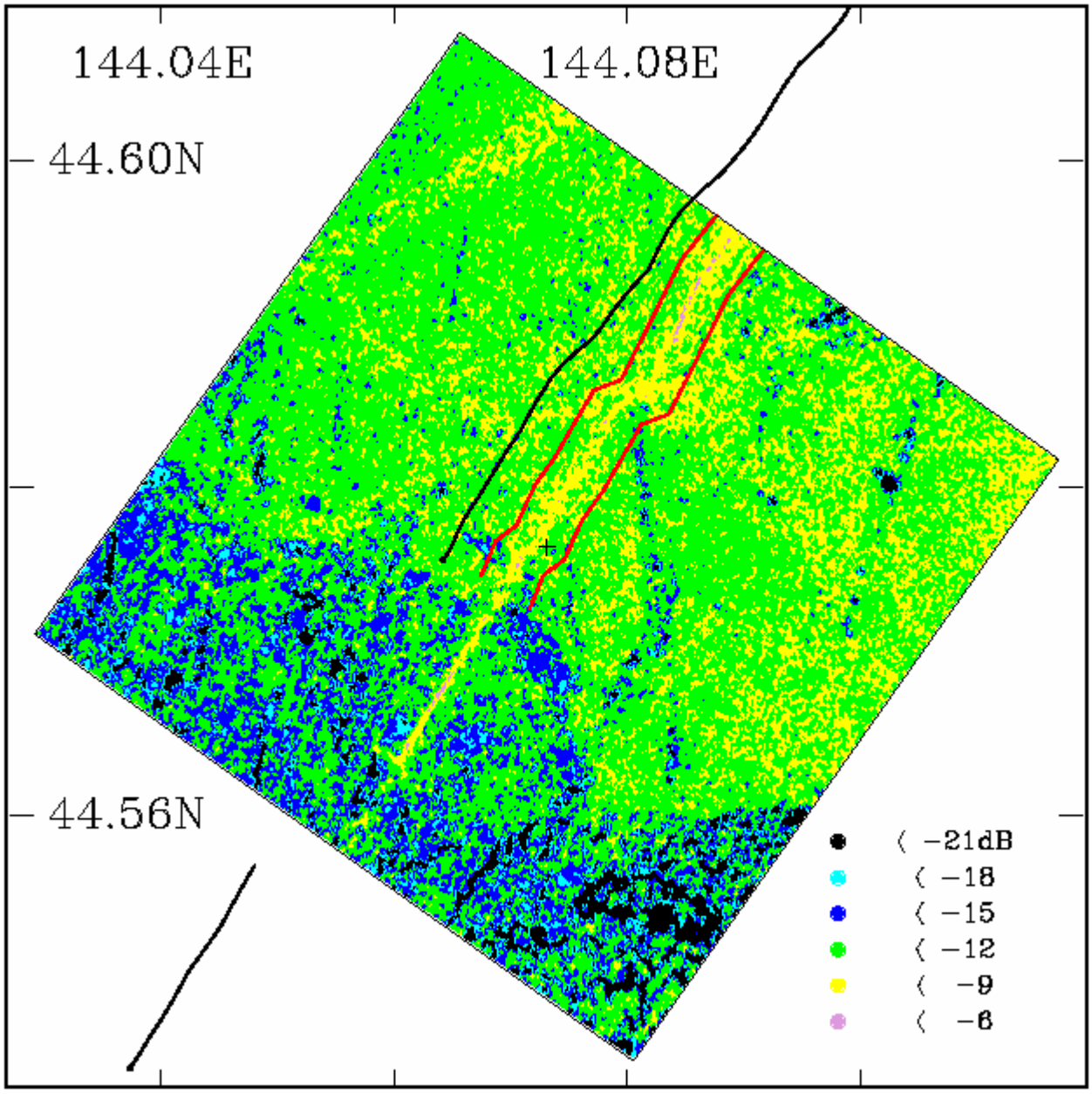

Figure 7. Distribution of backscattering coefficients in the square area of figure1, corresponding to No.5 in table 1.
The side length of the square is 5 km. Black lines are the ship track recorded with a ship-borne GPS. Note that this line slightly deviated from the line of high backscattering coefficients, showing sea ice drifted southward by the time of SAR observation. Red lines, taken 200 m away from the true ship track, were used for validation.

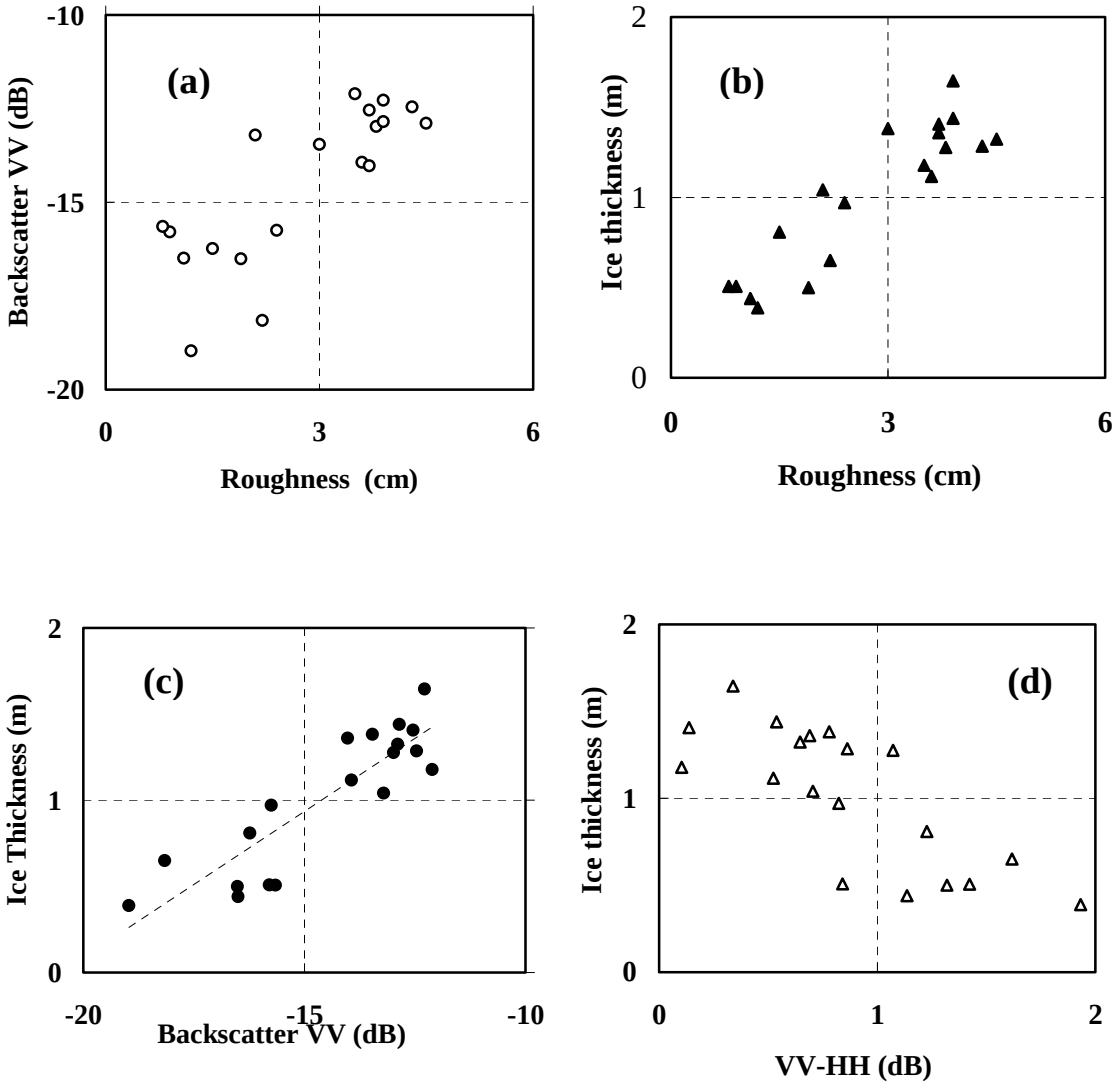

Figure 8. Scatter plots of the averaged values between

(a) Surface roughness and backscattering coefficient (VV)

(b) Surface roughness and ice thickness

(c) Backscattering coefficient (VV) and ice thickness

The regression is given by $y = 0.170\ x + 3.481$.

(d) Backscattering ratio (VV-HH) and ice thickness

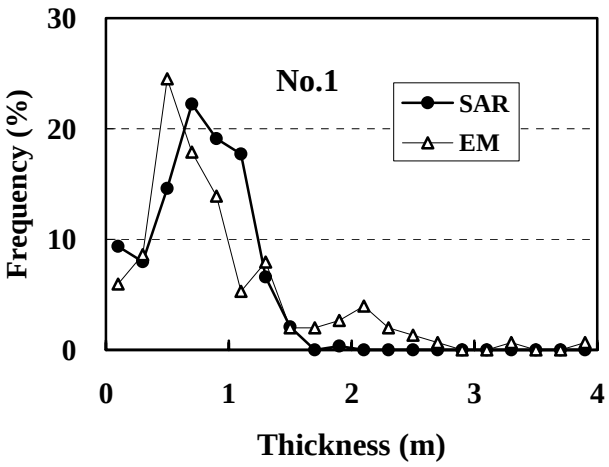
No.1
SAR
EM
Frequency (%)
Thickness (m)
0
10
20
30
0
1
2
3
4

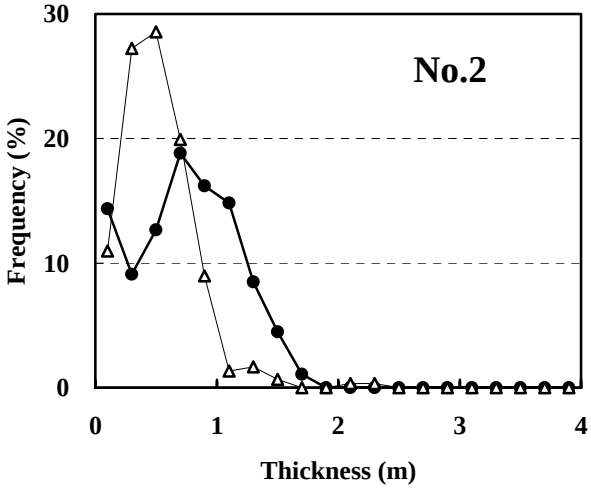
No.2
Frequency (%)
Thickness (m)
0
10
20
30
0
1
2
3
4

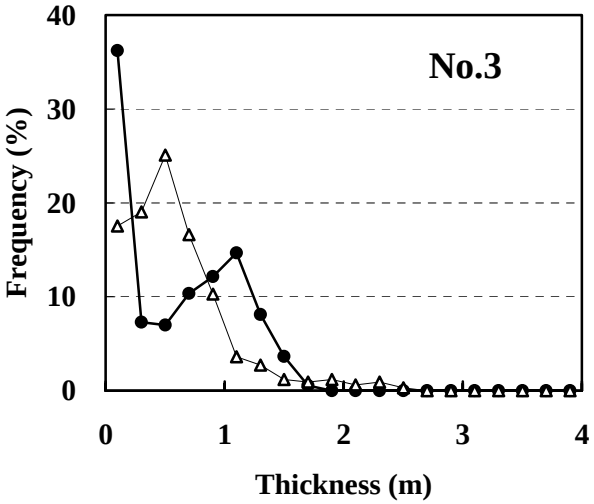
No.3
Frequency (%)
Thickness (m)
0
10
20
30
40
0
1
2
3
4

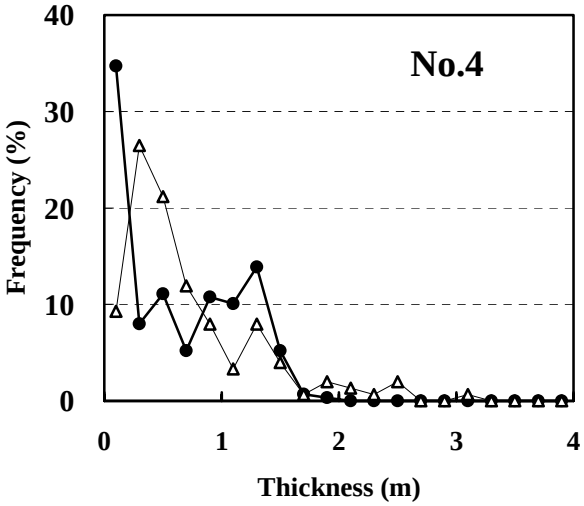
No.4
Frequency (%)
Thickness (m)
0
10
20
30
40
0
1
2
3
4

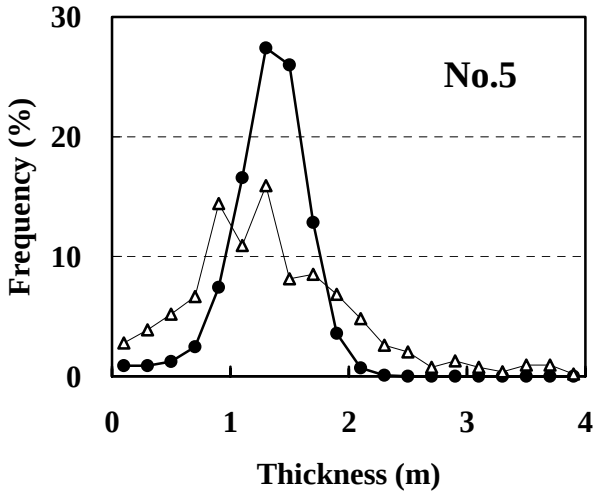
No.5
Frequency (%)
Thickness (m)
0
10
20
30
0
1
2
3
4

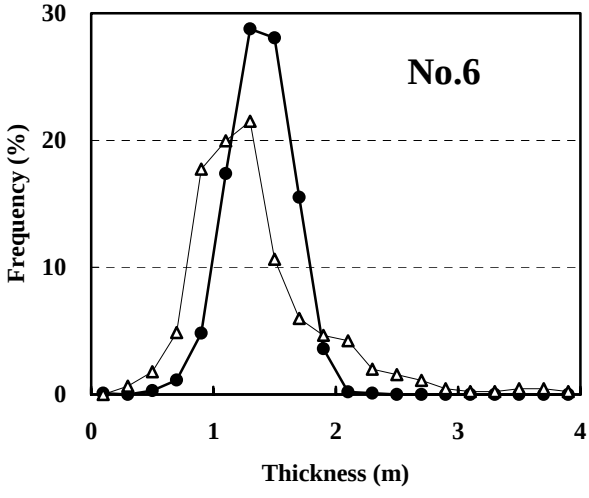
No.6
Frequency (%)
Thickness (m)
0
10
20
30
0
1
2
3
4

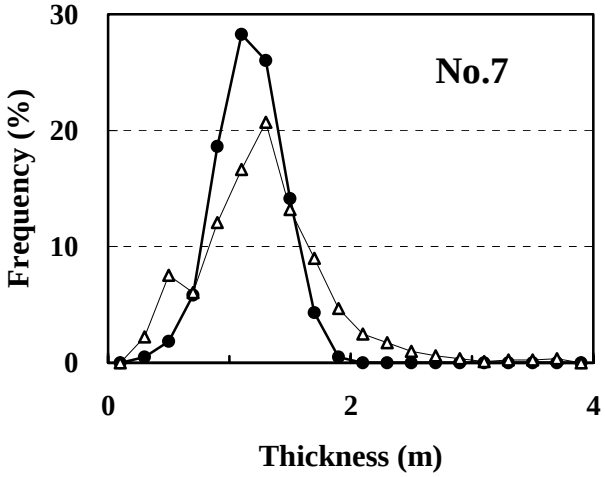

Figure 9. Ice thickness distribution along the individual selected observation lines.
Thick lines denote SAR-derived ice thickness with the regression in figure.8(c).
Thin lines denote EM-derived ice thickness distribution.

(a)

(b)

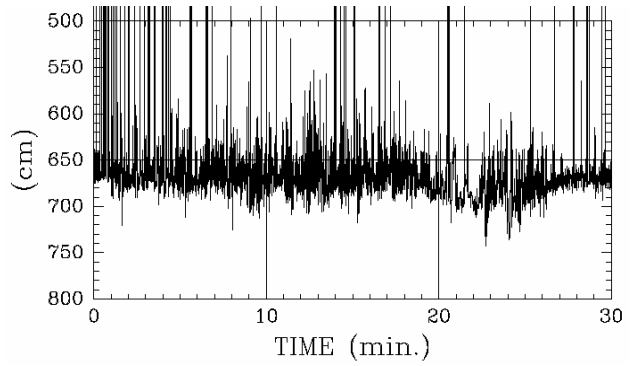

(c)

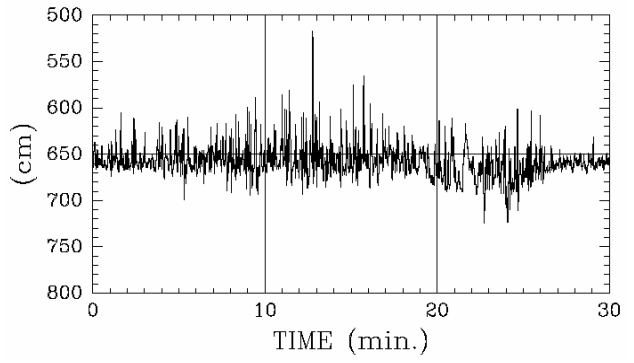

Figure 10. Comparison of the measurements between the supersonic and laser profilers, conducted in February 2006.

(a) Ice conditions of the exemplified area (09h05m LST on February 14, 2006).

(b) Example time series of the supersonic profiling data from 09h00m to 09h30m on February 14, 2006.

(c) Example time series of the laser profiling data during the same period.